J. Fluid Mech. (1986), *vol.* 167, *pp.* 309–326
Printed in Great Britain

Rotating hydraulics of flow in a parabolic channel

By KARIN BORENÄS AND PETER LUNDBERG
Department of Oceanography, University of Göteborg, Box 4038, S-400 40 Göteborg, Sweden

(Received 21 June 1985)

The investigation of Gill (1977) on the effects of a finite upstream depth upon frictionless flow through a rotating box-like channel has been extended to take into account a parabolic geometry. In addition to being more geophysically realistic, this type of topography with continuously sloping lateral boundaries has the advantage that it yields a unified solution. In contrast to the case of a rectangular channel, no separation of the geostrophically balanced downchannel flow from the sidewalls can take place. The resulting algebraic problem can be resolved either using an iterative technique or by the construction of perturbation series solutions. One of the most important results to emerge from the analysis is that the classical concept of hydraulic control is only applicable for a limited range of the parameters governing the problem. It is finally argued that this behaviour of the solutions is not due to the specific choice of geometry, but rather represents a common feature for all topographies characterized by a continuously sloping cross-stream bottom profile.

1. Introduction

Over the last few years there has been considerable interest in extending the framework of conventional hydraulic theory to also encompass the geophysically important effect of the rotation of the Earth. A major reason for this is that the deeper regions of the ocean are partitioned by submarine ridges into semiconnected basins and that recent field observations (cf. Hogg *et al.* 1982; Stalcup, Metcalf & Johnson 1975) indicate that some type of hydraulic control may constrain the geostrophic flow of dense bottom water through the deepest passages between the various basins.

Even though the effect of rotation upon the formation of hydraulic jumps had been considered previously by Houghton (1969), the first investigation to deal specifically with hydraulically critical rotating flow was reported in a paper by Stern (1972). A number of studies (cf. Whitehead, Leetma & Knox 1974; Stern 1974; Sambuco & Whitehead 1976) followed, which, in addition to formulating the problem in terms of a two-layer flow with a quiescent upper layer, made use of the geophysically somewhat unrealistic assumption of an infinite upstream depth. This disquieting feature of the models was redressed by Gill (1977), who allowed for a non-zero upstream potential vorticity due to a finite depth of the basin. (Interesting extensions of these latter results are due to Røed 1980, who examined inertial boundary currents, and to Hogg 1983, who considered a four-layer flow with application to deep-water conditions in the Vema Channel.)

Gill focused his attention upon a box-like channel, which necessitates a two-regime treatment of the problem, dependent on whether the geostrophically balanced down-channel flow is separated from the sidewall or not. (Note that although the analysis due to Shen (1981) formally took into account the effects of a lateral bottom topography, the upstream depth was assumed infinite and furthermore a channel with

vertical sidewalls was used in the laboratory experiments.) However, as pointed out by Gill (1977), his formulation of the problem can in principle be extended to also deal with the case of a continuously sloping bottom (whereby no distinction can be made between the sidewalls and the bottom boundary of the channel), and this is precisely what will be attempted in the present investigation.

In §2 the governing equations for the open-channel problem with a parabolic bottom profile will be discussed, and a set of transcendental equations for the points of intersection between the free surface of the fluid and the bottom will be derived. As will be shown in §§3 and 4, these equations cannot only be manipulated to yield an implicit equation for a uniquely defined flow variable, but they can also be resolved by the construction of power series solutions, formally valid in the limit of a channel width much smaller than the Rossby radius of deformation. In the following section the results, and in particular the controlled-flow solutions, will be discussed from a physical standpoint with a certain emphasis on factors limiting the usefulness of the present approach. A direct comparison with the results of Gill, in addition to an outline of the prospects for future work in the field, is undertaken in the final section.

2. Governing equations

The stationary, shallow-water flow to be considered is of a homogeneous, inviscid fluid in a rotating channel of parabolic cross-sectional bottom profile with the y-direction downstream. The velocity components in the x- and y-directions are u and v respectively. Figure 1 shows the geometrical notation, where the reference level ($z = 0$) is taken to be the highest elevation of the channel floor. The position of the bottom with regard to this level ($z = -h(x, y)$) is given by:

$$h(x, y) = \beta(y) - \alpha(y)\, x^2. \tag{2.1}$$

As is usual in hydraulics it will be assumed that all downstream variations of dynamical as well as topographical variables occur on a much larger scale than the width of the channel ($\partial/\partial x \gg \partial/\partial y$). The coordinates of the points of intersection between the free surface ($z = \eta$) of the fluid (of total depth $D = h + \eta$) and the boundary are denoted by $x = -a$ and $x = b$. (In a two-layer formulation of the problem, $z = \eta$ is the position of the interface between a lower layer of density ρ and a passive upper layer of density $\rho - \Delta\rho$.)

By use of scaling arguments based on the assumption of small down-channel variations of the flow it can be demonstrated that the cross-stream component of the momentum equation is reduced to the geostrophic equation for v:

$$fv = g \frac{\partial \eta}{\partial x}. \tag{2.2}$$

Here f is the Coriolis parameter and g, the acceleration due to gravity, is taken reduced ($g' = g\,\Delta\rho/\rho$) when considering the two-layer problem. A stream function Ψ is defined such that

$$Du = -\frac{\partial \Psi}{\partial y}; \quad Dv = \frac{\partial \Psi}{\partial x}; \quad \Psi(-a) = -\tfrac{1}{2}Q; \quad \Psi(b) = \tfrac{1}{2}Q,$$

where Q is the total transport through the channel. For an inviscid flow the potential vorticity is conserved along streamlines:

$$\frac{f + \dfrac{\partial v}{\partial x}}{D} = G(\Psi). \tag{2.3}$$

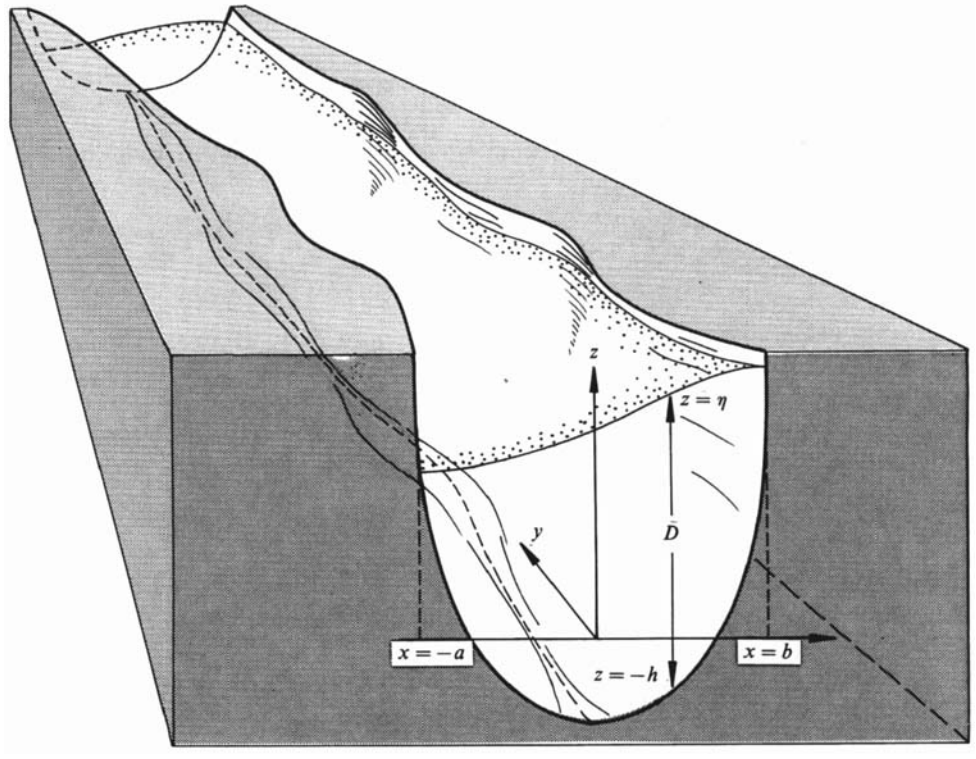

FIGURE 1. Definitional sketch showing the geometrical features of the channel.

If D_∞ is a characteristic upstream depth at points where the relative vorticity is zero, then the assumption that the potential vorticity G is uniform implies that $G = f/D_\infty$. The Bernoulli function $B(\Psi)$ is related to the potential vorticity by $G = \mathrm{d}B/\mathrm{d}\Psi$ and thus an integration yields

$$B(\Psi) = \frac{f\Psi}{D_\infty} + K,$$

where K is an as yet undetermined constant. Consequently the equation for the conservation of energy along a streamline becomes:

$$\eta g + \tfrac{1}{2}v^2 = \frac{f\Psi}{D_\infty} + K. \tag{2.4}$$

It is now postulated that the upstream basin has a rectangular cross-section and that it is very broad compared to $\lambda = (gD_\infty)^{\frac{1}{2}}/f$, the Rossby radius of deformation based on the upstream potential vorticity, i.e. the depth D_∞. In this case the upstream flow will take place adjacent to the vertical boundaries, thereby leaving the interior of the fluid motionless, and the constant of integration K can be determined in a straightforward manner by applying (2.4) to a streamline Ψ_1 emanating from the quiescent interior of the upstream region. For this streamline, $\eta = D_\infty - \beta_{\max}$, where $\beta_{\max}$ is the elevation of the highest point in the channel ($z = 0$) relative to the upstream bottom level, and thus $K = (D_\infty - \beta_{\max})g - f\Psi_1/D_\infty$. Bernoulli's equation assumes the following form:

$$\eta g + \tfrac{1}{2}v^2 = \frac{f(\Psi - \Psi_1)}{D_\infty} + (D_\infty - \beta_{\max})g. \tag{2.5}$$

Equations (2.1)–(2.3) yield an ordinary differential equation for η:

$$\frac{\partial^2\eta}{\partial x^2}-\frac{1}{\lambda^2}\eta+\frac{1}{\lambda^2}(D_\infty-\beta+\alpha x^2)=0.$$

Using the boundary conditions $D(-a)=D(b)=0$, the solution of this equation is found to be

$$\eta=\frac{(D_\infty+2\alpha\lambda^2)}{\sinh\left(\frac{a+b}{\lambda}\right)}\left[\sinh\left(\frac{x-b}{\lambda}\right)-\sinh\left(\frac{x+a}{\lambda}\right)\right]+D_\infty+2\alpha\lambda^2+\alpha x^2-\beta,$$

whereby the velocity $v(x)$ can be calculated from equation (2.2). Bernoulli's equation (2.5) can now be evaluated at the points of intersection between the free surface and the solid boundary, yielding two implicit equations for the dependent variables a and b. This set of equations is non-dimensionalized by introducing the following length and velocity scales:

$$\lambda=\frac{(gD_\infty)^{\frac{1}{2}}}{f};\quad D_s=\left(\frac{fQ}{g}\right)^{\frac{1}{2}};\quad V_s=\left(\frac{fQ}{D_\infty}\right)^{\frac{1}{2}}.$$

This scaling satisfies continuity, $Q=\lambda D_s V_s$, as well as the geostrophic relationship (2.2), $\lambda f V_s=gD_s$. The equations for $a^*=a/\lambda$ and $b^*=b/\lambda$ turn out to be:

$$a^{*2}=r\left(1-\frac{\Delta}{\hat{D}_\infty}\right)-\frac{r}{\hat{D}_\infty^2}(\hat{\Psi}_i+\tfrac{1}{2})-\frac{1}{2r}\left((2+r)\tanh\left(\frac{a^*+b^*}{2}\right)-2a^*\right)^2, \tag{2.6a}$$

$$b^{*2}=r\left(1-\frac{\Delta}{\hat{D}_\infty}\right)-\frac{r}{\hat{D}_\infty^2}(\hat{\Psi}_i-\tfrac{1}{2})-\frac{1}{2r}\left((2+r)\tanh\left(\frac{a^*+b^*}{2}\right)-2b^*\right)^2. \tag{2.6b}$$

(For notational convenience, stars will henceforth be dropped.) The problem is governed by the following dimensionless quantities:

$$\Delta=\frac{(\beta_{\max}-\beta)}{D_s};\quad r=\frac{f^2}{g\alpha};\quad \hat{D}_\infty=\frac{D_\infty}{D_s};\quad \Psi_i=\frac{\hat{\Psi}_i}{Q}.$$

Here Δ and r are geometrical parameters, the former being the non-dimensional height of the channel floor above the upstream level, whereas the latter is the second power of the dimensionless width of the channel. $\hat{D}_\infty$ is a non-dimensional measure of the upstream depth and $\hat{\Psi}_i$ specifies the distribution of the volume flux far upstream between the boundary layers adjacent to the sidewalls of the basin. (Observe that the three dimensional quantities D_∞, Ψ_i, and Q necessary to characterize the upstream flow have been reduced to the two dimensionless parameters $\hat{D}_\infty$ and $\hat{\Psi}_i$ since the vertical lengthscale is based on the volume flux.) The governing equations are symmetric in (a,b), and hence they can represent an overall flow in the positive as well as negative y-direction. In what follows we shall, however, be solely concerned with a total transport in the direction of the positive y-axis, i.e. $b>a$.

Since equations (2.6a,b) are transcendental as well as implicit, the most straightforward method of solution proved to be an iterative procedure, the results of which will be summarized in the next section. However, as will be shown in §4, it is also possible to construct explicit analytical solutions to the problem, based upon perturbation expansions valid in the limit of small r.

Note finally that, in view of the forthcoming representation of the solutions, it proves convenient to express the results in terms of a uniquely defined and physically meaningful flow variable, which is taken to be the cross-sectional area A occupied

by the flow. By integrating the total depth D cross-stream and making use of the difference between equation (2.6a) and (2.6b), it is found that:

$$A = r[\hat{D}_\infty(b-a)]^{-1},$$

where A has been non-dimensionalized with respect to λD_s.

3. Iterative solution

Subtracting (2.6a) from (2.6b) one obtains:

$$(b-a) = r^2\left[\hat{D}_\infty^2(2+r)\left((a+b)-2\tanh\left(\frac{a+b}{2}\right)\right)\right]^{-1}. \tag{3.1}$$

Insertion of this expression in the sum of the two governing transcendental equations results in an implicit relationship for $(a+b)$:

$$(2+r)\left((a+b)-2\tanh\left(\frac{a+b}{2}\right)\right)^2\left[(2+r)(a+b)^2+4r^2\left(\frac{\hat{\Psi}_i}{\hat{D}_\infty^2}-1+\frac{\Delta}{\hat{D}_\infty}\right)\right.$$
$$\left.+2(2+r)^2\tanh^2\left(\frac{a+b}{2}\right)-4(a+b)(2+r)\tanh\left(\frac{a+b}{2}\right)\right]+\left(\frac{r}{\hat{D}_\infty}\right)^4=0, \tag{3.2}$$

which is solved numerically using for instance the secant method. Thus $(a+b)$ can be determined for prescribed values of $\hat{\Psi}_i$, $\hat{D}_\infty$, r, and Δ, whereafter use of equation (3.1) yields A and (a, b). The numerical results reported in this section are for the case of $\hat{\Psi}_i = \frac{1}{2}$. This corresponds to a situation with the flow in the upstream basin being concentrated in a unidirectional boundary layer adjacent to the left bank relative to the direction of the overall flow. (For a detailed justification of this particular choice of upstream conditions cf. Gill 1977.) Note furthermore that the entire regime $-\frac{1}{2} \leqslant \hat{\Psi}_i \leqslant +\frac{1}{2}$ is one of no upstream flow reversals.

Figure 2 pertains to the case of a fixed value of Δ (here $\Delta = 0$), i.e. the level of the channel floor is unchanged downstream, whereas the degree of horizontal contraction of the passage, as measured by the parameter r, is varied. The results in terms of a rescaled cross-sectional area $A/r^{\frac{1}{2}}$ versus $\log_{10} r$ are shown for various values of $\hat{D}_\infty$. The graph demonstrates that, given $\hat{D}_\infty$, the solution of (3.2) consists of two branches which emerge for a certain value of r. In a similar fashion, but for a fixed value of r (here $r = 1$), figure 3 shows $A/r^{\frac{1}{2}}$ versus $\Delta/\hat{D}_\infty$. This latter variable is the ratio of the height of the channel floor above the upstream level to the upstream depth D_∞. The degree of constriction encountered by the flow is in this case directly proportional to $\Delta/\hat{D}_\infty$, whereas in figure 2 it has an inverse relationship to the magnitude of r, hence the mirrored quality of the two graphs.

Even though a discussion of the physical basis of these results is deferred until §5, an interpretation of the graphs, conforming to the maximization principle of non-rotating hydraulics, can be formulated as follows. Let the dimensional upstream depth D_∞ be prescribed as well as the geometrical parameter r^* (or Δ^*) characterizing the narrowest (or most shallow) section of the channel. Then $\hat{D}_\infty(r^* \wedge \Delta^*)$, the magnitude of $\hat{D}_\infty$ associated with the solution curve which has its branch-point at this particular value r^* (or Δ^*), will represent the largest possible transport, $Q_{\max} = (D_\infty/\hat{D}_\infty(r^* \wedge \Delta^*))^2 g/f$, through the channel under the dynamical constraints outlined in the previous section. It is evident from figures 2 and 3 that once the dimensional upstream depth has been specified, all other possible solutions to the problem correspond to lower transports for the pertinent value of the geometrical parameter.

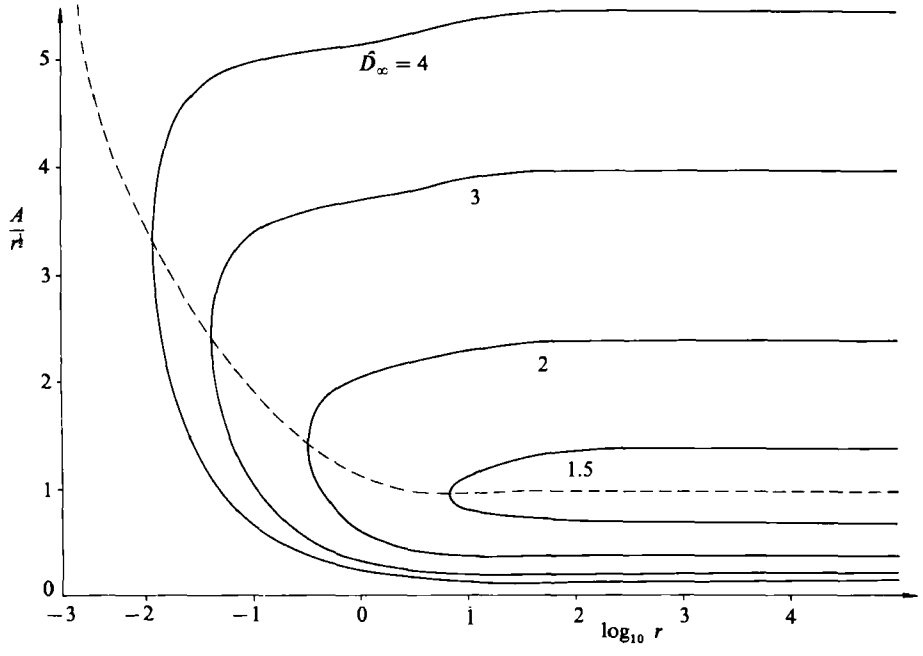

FIGURE 2. $A/r^{\frac{1}{2}}$ versus $\log_{10} r$ for various values of $\hat{D}_\infty$ when $\Psi_1 = \frac{1}{2}$ and $\Delta/\hat{D}_\infty = 0$. The dashed line indicates the position of the branch-point.

By examining the properties of a long-wave disturbance on the flow, a slightly non-standard Froude number can be defined as $F = \bar{v}/(\bar{v}-c)$, where $\bar{v} = \frac{1}{2}(v(-a)+v(b))$ and c is the celerity of the long-wave disturbance. This weak definition of the average velocity $\bar{v}$ is a prerequisite for the derivation of an explicit expression for F. Note, however, that, for the parabolic bottom topography considered here, conventional averaging proves to be equivalent to the weak variety, i.e.

$$\tfrac{1}{2}(v(-a)+v(b)) = \frac{1}{(a+b)}\int_{-a}^{b} v(x)\,\mathrm{d}x.$$

By assuming a down-channel scale of the disturbances much larger than the cross-stream scale, yet small with regard to the lengthscale of the downstream variations of the topography, and furthermore positing an unchanged potential vorticity of the disturbed flow (cf. Gill 1977), the following expression for F can be derived:

$$F^{-2} = \left(\frac{\hat{D}_\infty}{r}\right)^4 (2+r)^2 \left((a+b) - 2\tanh\left(\frac{a+b}{2}\right)\right)^2 \left[\left((a+b) - (2+r)\tanh\left(\frac{a+b}{2}\right)\right)^2 + 2r(a+b)\coth(a+b) - 2r - r(2+r)\tanh^2\left(\frac{a+b}{2}\right)\right]. \quad (3.3)$$

From hydraulic theory it is not surprising that the branch-points of figures 2 and 3 prove to be characterized by $F = 1$, whereas $F < 1$ and $F > 1$ for the upper and lower branches respectively of the solution curves, a state of affairs that will be considered in greater detail in §5.

To conclude this section on the formal aspects of the solution to the problem it might be remarked that an alternative method, requiring no physical insight, of

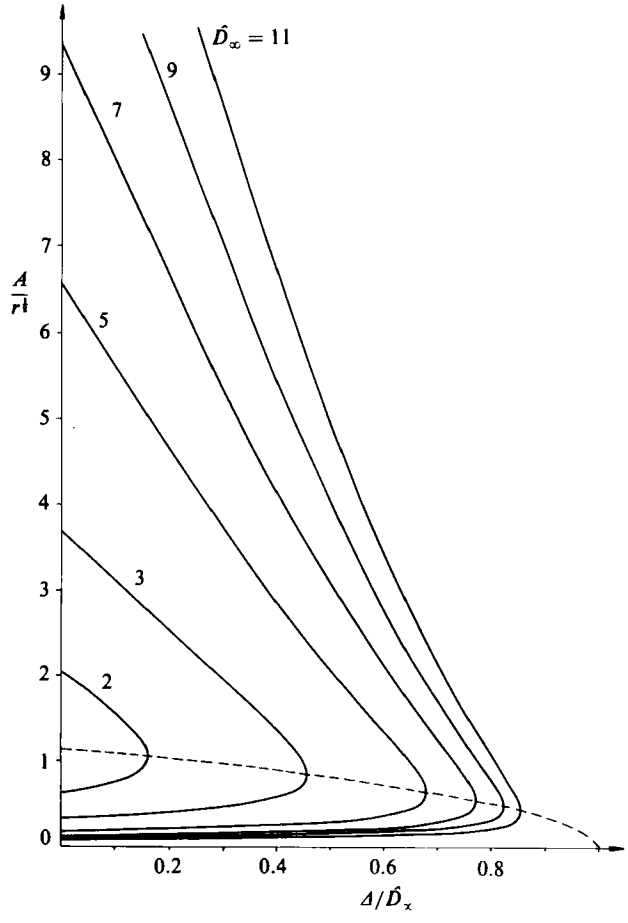

FIGURE 3. As in figure 2, but for $A/r^{\frac{1}{2}}$ versus $\Delta/\hat{D}_\infty$ when $\hat{\Psi}_1 = \frac{1}{2}$ and $r = 1$.

characterizing the point where the two solution branches coalesce, is to recognize that from (3.2), $(a+b)$ is implicitly determined, $\mathscr{G}(a+b, \Delta, r, \hat{D}_\infty, \hat{\Psi}_1) = 0$. Thus, from the implicit function differentiation theorem, it is found that the unique solution is distinguished by:

$$\frac{\partial \mathscr{G}(a+b, \Delta, r, \hat{D}_\infty, \hat{\Psi}_1)}{\partial(a+b)} = 0.$$

This expression is, as indeed can be verified by some algebraic manipulation, precisely equivalent to (3.3) with $F = 1$.

4. Perturbative solution

From figure 2 it is evident that given $\hat{D}_\infty$, any attempt to expand the solutions of equations (2.6a, b) in powers of r will be futile since the problem has no real roots for r smaller than the value associated with the branch-point. The formal source of this failure of the conventional technique can be traced to the symmetry-breaking terms $r(\hat{\Psi}_1 \pm \frac{1}{2})/\hat{D}_\infty^2$ of the governing equations, which, for expansions of a and b in any fractional power of r, give rise to inconsistent results already to lowest order.

The problem, however, becomes amenable to perturbation analysis by observing that $\hat{D}_\infty$, which hitherto has been regarded as autonomous, is dependent upon the Coriolis parameter f and hence can be rescaled invoking r:

$$\hat{D}_\infty^{-2} = \mu r^{\frac{1}{2}}.$$

Use of this relationship in conjunction with the transformed variables $(a', b') = r^{-\frac{1}{2}}(a, b)$ yields a regular perturbation problem well adapted for an expansion in powers of $r^{\frac{1}{2}}$, a quantity which for convenience will be denoted p. Furthermore, by recognizing that $\Delta/\hat{D}_\infty$, the ratio of the threshold height to the upstream depth, is independent of f and consequently not affected by the rescaling above, the governing equations for the new variables (a', b') assume the following form:

$$2p^2a^2 = 2p^2\left(1-\frac{\Delta}{\hat{D}_\infty}\right) - 2p^3\mu(\hat{\Psi}_1+\tfrac{1}{2}) - ((p^2+2)\,[C_1(a+b)+C_3p^2(a+b)^3+\ldots]+2a)^2, \tag{4.1a}$$

$$2p^2b^2 = 2p^2\left(1-\frac{\Delta}{\hat{D}_\infty}\right) - 2p^3\mu(\hat{\Psi}_1-\tfrac{1}{2}) - ((p^2+2)\,[C_1(a+b)+C_3p^2(a+b)^3+\ldots]+2b)^2. \tag{4.1b}$$

Here the primes have been dropped and the hyperbolic tangent has been expanded in a MacLaurin series, convergent for $|a+b| < \pi$:

$$\tanh\left(\frac{a+b}{2}\right) = -\sum_{u=1}^{\infty} C_{2k-1}(a+b)^{2k-1}; \quad C_{2k-1} = \frac{-2(2^{2k}-1)}{(2k)!}\,B_{2k}.$$

B_n is the nth Bernoulli number, readily generated from:

$$x/(\mathrm{e}^x-1) = \sum_{n=0}^{\infty} B_n x^n/n!.$$

By inserting the solutions in power series form,

$$(a, b) = \sum_{k=0}^{\infty} (a_k, b_k)\,p^k,$$

and ordering in powers of p, the governing equations can be resolved to any desired order. Experience has, however, revealed that for practical purposes it is most convenient to base the ordering procedure on the sum of and difference between equations (4.1a) and (4.1b), and in what follows the results to order N derived from these linear combinations of the governing equations will be designated $\sigma(N)$ and $\delta(N)$ respectively. The equations obtained for $N \leqslant 5$ assume the following form:

$$\delta(0)\text{: } —, \qquad \delta(1)\text{: } —, \quad \delta(2)\text{: } —,$$

$$\sigma(0)\text{: } a_0 = b_0, \quad \sigma(1)\text{: } —, \quad \sigma(2)\text{: } (a_1-b_1)^2 = 2\left(1-\frac{\Delta}{\hat{D}_\infty}-a_0^2\right),$$

$$\delta(3)\text{: } 2\mu+\tfrac{1}{3}(a_1-b_1)\,(a_0+b_0)^3 = 0,$$

$$\sigma(3)\text{: } \mu\hat{\Psi}_1+a_0(a_1+b_1)+(a_1-b_1)\,(a_2-b_2) = 0,$$

$$\delta(4)\text{: } (a_2-b_2)\,8a_0^3+12a_0^2(a_1-b_1)\,(a_1+b_1) = 0,$$

$$\sigma(4)\text{: } a_1^2+b_1^2+2a_0(a_2+b_2)+(a_2-b_2)^2+2(a_1-b_1)\,(a_3-b_3)+a_0^2 - 32a_0^4C_3+256a_0^6C_3^2 = 0,$$

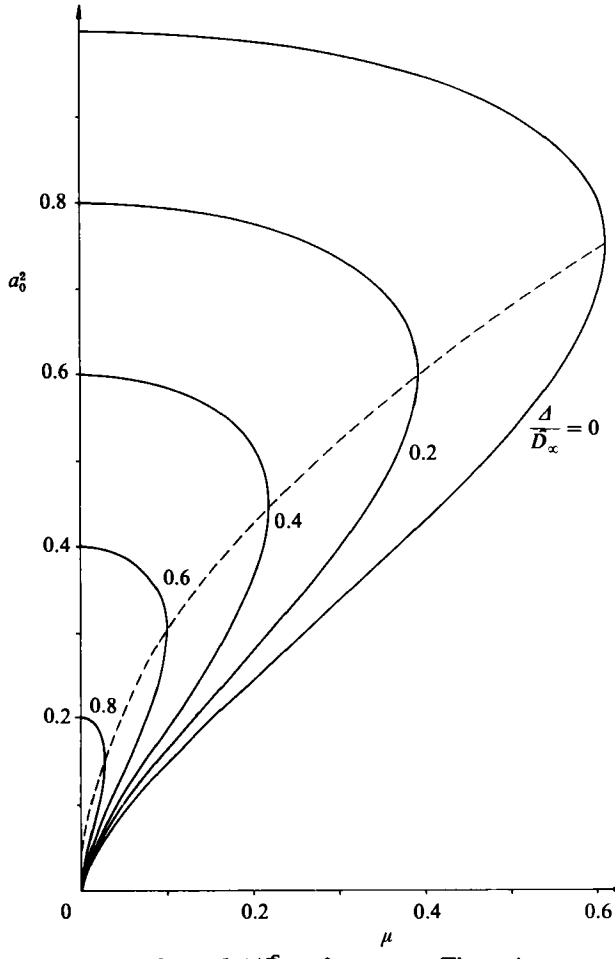

FIGURE 4. For various values of $\Delta/\hat{D}_\infty$, a_0^2 versus μ. The unique magnitude of a_0^2 for the maximum value of μ for each $\Delta/\hat{D}_\infty$ is shown as a dashed line.

$$\delta(5):\ (a_1-b_1)\,8a_0^3+2(a_1-b_1)\,[6a_0(a_1+b_1)^2+12a_0^2(a_2+b_2)]$$
$$+2(a_2-b_2)\,12a_0^2(a_1+b_1)+2(a_3-b_3)\,8a_0^3+2\,\frac{C_5}{C_3}\,(a_1-b_1)\,32a_0^5=0,$$

$$\sigma(5):\ 2a_0(a_3+b_3)+2a_1a_2+2b_1b_2+2(a_1-b_1)\,(a_4-b_4)+2(a_2-b_2)\,(a_3-b_3)$$
$$+a_0(a_1+b_1)-2C_3(a_1+b_1)\,32a_0^3+4C_3^2(a_1+b_1)\,6\times32a_0^5=0.$$

(The general recursive formulae for $\sigma(N)$ and $\delta(N)$, $N\geqslant 6$, are stated in the Appendix.)

Use of $\delta(3)$ and $\sigma(2)$ yields an equation for a_0 in terms of $\Delta/\hat{D}_\infty$ and μ:

$$a_0^8-\left(1-\frac{\Delta}{\hat{D}_\infty}\right)a_0^6+\tfrac{9}{36}\mu^2=0.$$

Since this equation is symmetric in a_0 (corresponding to flow in the positive or negative y-direction), figure 4 shows the real roots a_0^2 versus μ for various values of the topographical parameter $\Delta/\hat{D}_\infty$. (Complex-conjugate roots have been omitted since they are of no physical interest.) From the graph it is evident that the real

solutions in general are bi-valued, with each of the a_0 serving as the 'seed' for one of the solution branches of figures 2 and 3. An algebraic calculation shows that these roots a_0 coalesce for

$$\mu^{\frac{1}{2}} = (\tfrac{3}{8})^{\frac{1}{4}} \left(1 - \frac{\Delta}{\hat{D}_\infty}\right), \tag{4.2}$$

yielding $a_0^2 = 3(1-\Delta/\hat{D}_\infty)/4$. The position of this branch-point is shown in the diagram as a dashed line. These unique solutions correspond to controlled-flow situations in the non-rotating analogue to the problem at hand. Most easily this can be perceived by rewriting (4.2) in dimensional form:

$$Q = \left(\frac{3g}{8\alpha}\right)^{\frac{1}{2}} (D_\infty - \beta)^2,$$

which proves to be precisely the expression obtained by maximizing the total flow in a non-rotating parabolic channel under the constraints of volume and energy conservation.

The values of a_0 having been determined, solutions valid to any order can be generated. The overall structure of the recursive formulae is such that once $\delta(N)$, $\sigma(N)$, and $\delta(N+1)$ are known, the problem is fully resolved to order $N-2$ in addition to providing $(a_{N-1}-b_{N-1})$, a useful quantity in view of the flow variable A defined in §2. For small values of the expansion parameter even results of comparatively low order can be useful, as illustrated in figure 5. In a similar manner as in figure 2, but here for A versus r, this graph shows the region in the immediate vicinity of the branch-point for $\hat{D}_\infty^2 = 8$, where the solid line represents the solution calculated using the methods of the preceding section. The dotted, dashed and dot–dashed lines show the truncated series solutions consisting of four, seven and ten terms respectively. The perturbation expansions have been computed locally in r for $\mu = 1/(8r^{\frac{1}{2}})$ and the two solution branches, each corresponding to one of the values of a_0, are clearly in evidence. The diagram moreover indicates that for r smaller than the value associated with the branch-point the perturbation series diverge, whereas for larger values of r they converge towards the proper solutions. This behaviour, arising from the non-uniform convergence of the series due to the parameter μ, in essence constitutes the mechanism whereby the perturbation expansion can cope with the previously noted circumstance that real solutions to the problem only emerge for a finite value of r.

When discussing the overall applicability of the perturbation expansions derived here, the convergence of these power series in r should be formally investigated for a fixed value of the parameter $\mu = 1/(\hat{D}_\infty^2 r^{\frac{1}{2}})$. This quantity was, however, introduced solely with the aim of regularizing the problem, and thus in itself lacks physical interest except when considered in conjunction with a fixed value of the expansion parameter r. Since we are primarily interested in the series for computational purposes, an operational 'definition' of the radius of convergence as regards r was adopted, based upon whether or not the series expansions of the two solution branches converged for a fixed value of $\hat{D}_\infty$.

Inasmuch as the power series proved to converge for the entire range of parameter values considered in figure 3, interest was directed towards the situation depicted in figure 2 ($\hat{D}_\infty$ and r varying for a fixed value of Δ), and in particular on whether the branch-points could be accurately represented as the intersection between the two branches of the series solutions. (This choice of focal point for the convergence investigations was dictated partly by the branch-point being of great physical interest, partly by experience having revealed that a breakdown of the series

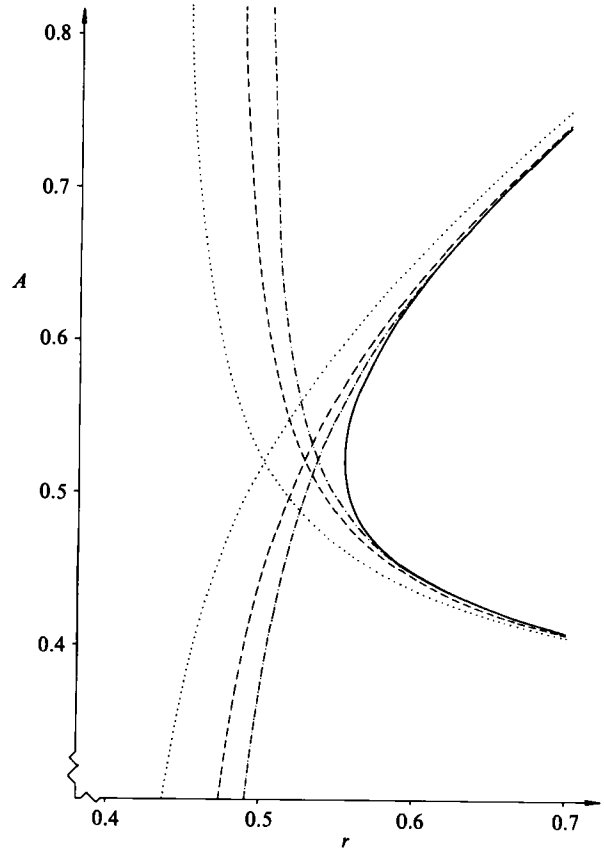

FIGURE 5. The iterative solution (solid line) near the branch-point for $\hat{D}_\infty^2 = 8$, $\hat{\Psi}_1 = \frac{1}{2}$, and $A/\hat{D}_\infty = 0$. The dotted, dashed and dot–dashed lines show the results from four-, seven- and ten-term power series approximations respectively.

expansions for a fixed value of $\hat{D}_\infty$ is first signalled here.) It was found that for $\hat{D}_\infty > 1.7$ (corresponding to small values of the expansion parameter r since this latter quantity for the branch-point is inversely proportional to the magnitude of $\hat{D}_\infty$ as evidenced by figure 2), an accuracy varying between ten and four places was obtained when the series were truncated after 51 terms. For $\hat{D}_\infty = 1.6$ ($r = 1.98$) the convergence shows signs of faltering, with the 51-term series only yielding two correct digits, and for $\hat{D}_\infty = 1.55$ the series solutions diverge.

It has, however, been found that by use of Padé approximations the domains of validity of the power series under consideration here can be extended beyond their 'radii of convergence' for fixed values of $\hat{D}_\infty$. By recasting the fiftieth-order series polynomials for $\hat{D}_\infty = 1.55$, 1.525, and 1.5 (corresponding to branch-point values of r equal to 3.16, 4.49, and 6.73 respectively) in the form of rational fractions, the point of intersection between the two solution branches could be determined with two-place accuracy from the diagonal [25, 25] Padé approximations. In a strict sense it is not meaningful to attempt to relate the accuracy of these results to the magnitude of the expansion variable r since the convergence of the perturbation series is non-uniform. From the standpoint of applications it can nevertheless be worthwhile to record that the relative error, although remaining of the order of 1 %, increased for larger branch-point values of r.

It may furthermore be noted that diagnostic computations indicate that, at least for the range of parameters considered here, it is not the radius of convergence of the power-series representation of the hyperbolic tangent (limited by a singularity on the real r-axis) which imposes the bounds on the applicability of the perturbation expansions outlined above. This conjecture, based upon purely numerical investigations, is further borne out by the neither fixed nor alternating sign patterns of the perturbation series, which indicate that their radii of convergence are determined by pairs of singularities at conjugate points in the complex r-plane (cf. Van Dyke 1974).

To conclude this section it may be appropriate to once again emphasize the interesting fact that it has proved possible to resolve by perturbation analysis an algebraic problem displaying singular characteristics in that real solutions are non-existent for small values of the perturbative quantity. This has been accomplished by a parameter rescaling invoking the expansion variable, whereby the resulting non-uniform convergence of the perturbation series does justice to precisely this feature of the solutions.

5. Results

Following established hydraulic procedure, the branch-points of figures 2 and 3 can tentatively be identified with controlled-flow situations yielding the maximum discharge for given upstream conditions and characterized by a Froude number of unity. The upper and lower solution branches represent sub- and supercritical flows respectively. For the parabolic bottom topography, the position of the control section is, for a given upstream depth, determined by the geometrical parameters r and Δ. From the point of view of the dynamics of the problem, the sole constraint on these latter quantities is that they be slowly varying in the downstream direction. Thus the overall conditions in any reasonably smooth channel of fundamentally parabolic cross-section can be calculated by prescribing r and Δ as functions of the downchannel coordinate and applying the methods of solution discussed in the preceding sections.

For the analogous problem when the channel has a rectangular cross-section it has been shown by Gill (1977) that the branch-point solution always represents a unidirectional velocity field. Consonant with the general notion of controlled flow, downstream conditions in this case neither through advection proper nor a long-wave signal can exert any influence upstream. When, however, as always in nature as well as for this investigation, the flow is delimited horizontally by a continuously sloping bottom, a radically different situation emerges, since in this case a branch-point solution is not necessarily associated with unidirectional flow even though the Froude number is equal to one. A qualitative insight into this phenomenon can be reached by examining (2.3), from which it is recognized that for the depth D approaching zero, as is the case at the horizontal extremes of the flow when the sidewalls are not vertical, the cross-stream gradient of the downchannel velocity $v(x)$ must be negative in order to conserve the prescribed upstream potential vorticity. Thus, for a sufficiently large, but finite, slope of the bottom where it intersects the free surface, the velocity may have to take recourse to a change of direction in order to fulfil one of the basic constraints of the theory. Should this be the case for the branch-point solution, then streamlines originating from the down-channel reservoir will pass the 'control section', a situation incompatible with the concept of an a priori specified upstream state. Hence it is not physically meaningful to invoke the notion of a controlled flow when the branch-point solution is associated with a flow reversal, and it furthermore

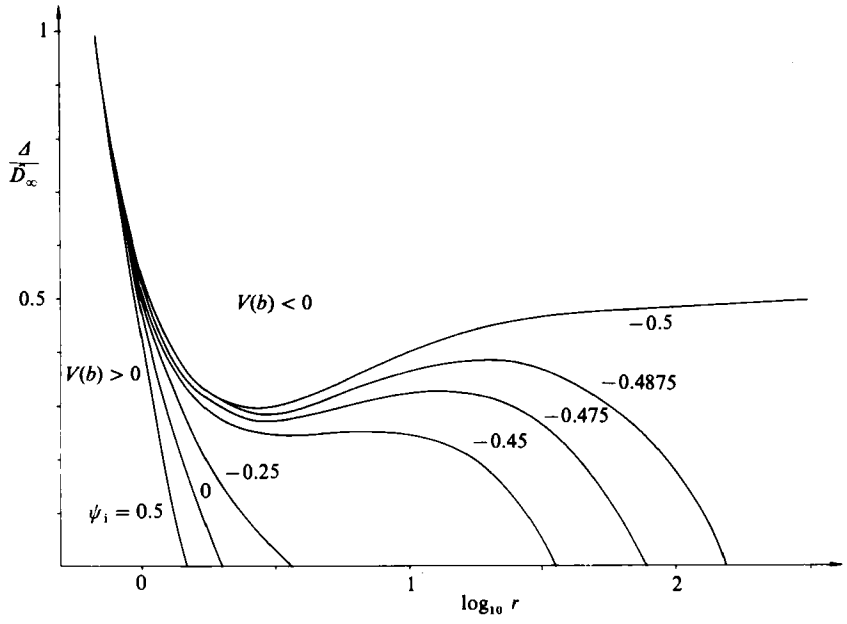

FIGURE 6. Curves yielding the specific combinations of branch-point values of r and $\Delta/\hat{D}_\infty$ for which the velocity on the right-hand side of the channel becomes negative. The results are shown for various values of $\hat{\Psi}_1$.

becomes of interest to establish criteria for the existence of a control section in the classical sense.

In the case of a parabolic bottom profile it can be proved for the branch-point solutions that if a reversal of the flow does take place, this must occur adjacent to the right-hand boundary of the channel. (This formal property of the velocity field is established by first disproving the existence of an interior flow reversal, i.e. showing that there is no point $x_0 \in (-a, b)$ such that the velocity $v(x)$ has a non-positive proper minimum characterized by $v'(x_0) = 0$ and $v''(x_0) > 0$. From (2.3) it is recognized that $v'(-a) < 0$, and consequently also a flow situation with $v(-a) < 0$ is excluded.) It may be noted that this state of affairs conforms to intuitive expectations in that the geostrophically induced asymmetry of the free surface leads to the largest values of the bottom slope being encountered by the flow on the extreme right-hand side of the channel. The construction of a diagram, delimiting the parameter regimes where the branch-point solutions to the present problem correspond to controlled flows in the classical sense, becomes a straightforward matter, and the results are summarized in figure 6. Shown here is a parameter space constituted by the branch-point values of r and $\Delta/\hat{D}_\infty$. For various $\hat{\Psi}_1 \in [-\frac{1}{2}, +\frac{1}{2}]$, i.e. for a uni-directional upstream flow, the plane is partitioned into a lower, left-hand region where the branch-point solutions do not admit any flow reversals ($v(b) \geqslant 0$), as well as a clime beyond the reaches where the established concept of a control section makes sense ($v(b) < 0$). Note that the graph conveys no information about $\hat{D}_\infty$ for the branch-point solutions, it only demonstrates whether or not a physically meaningful controlled-flow solution can be realized. Inasmuch as $\Delta/\hat{D}_\infty \to 1$ represents the limiting case of an infinite upstream depth it is not surprising that the separating curves of the graph coalesce here, since in this case the upstream potential vorticity is zero and a degenerate problem, independent of $\hat{\Psi}_1$, arises.

The qualitative traits of figure 6 in the limit of large r can be understood in terms of the asymptotic behaviour of the governing equations (2.6a, b). By transforming the dependent variables, $(a, b) = r^{\frac{1}{2}}(a', b')$, and making use of the one-sided MacLaurin expansion,

$$\tanh\left(\frac{1}{[\frac{1}{2}r^{\frac{1}{2}}(a'+b')]^{-1}}\right) = 1+0\times([\tfrac{1}{2}r^{\frac{1}{2}}(a'+b')]^{-1})^1 + 0\times([\tfrac{1}{2}r^{\frac{1}{2}}(a'+b')]^{-1})^2+\ldots \quad \text{as } [\tfrac{1}{2}r^{\frac{1}{2}}(a'+b')]^{-1}\to{}^{+}0,$$

it is found that in the limit of r approaching infinity the equations decouple with the following analytical solutions for the original variables:

$$a = 1\pm\left[-\tfrac{1}{2}r+\frac{r^2}{(2+r)}\left(1-\frac{\Delta}{\hat{D}_\infty}-\frac{1}{\hat{D}_\infty^2}(\hat{\Psi}_1+\tfrac{1}{2})\right)\right]^{\frac{1}{2}}, \tag{5.1a}$$

$$b = 1+\left[-\tfrac{1}{2}r+\frac{r^2}{(2+r)}\left(1-\frac{\Delta}{\hat{D}_\infty}-\frac{1}{\hat{D}_\infty^2}(\hat{\Psi}_1-\tfrac{1}{2})\right)\right]^{\frac{1}{2}}. \tag{5.1b}$$

Here the square root in the expression for a is taken positive for the subcritical solution branch, negative in the case of a supercritical flow. (Note that the choice of expanding the hyperbolic tangent for a large positive value of the argument has reduced the problem to one of an overall flow in the positive y-direction.) The formulae above for a and b demonstrate that, given a large enough value of r, the branch-point is characterized by

$$-\tfrac{1}{2}r+\frac{r^2}{(2+r)}\left(1-\frac{\Delta}{\hat{D}_\infty}-\frac{1}{\hat{D}_\infty^2}(\hat{\Psi}_1+\tfrac{1}{2})\right) = 0, \tag{5.2}$$

in which case $b = 1+r/(\hat{D}_\infty(2+r)^{\frac{1}{2}})$. Using the expansion above, the limiting form of the velocity distribution can also be calculated and it is recognized that

$$v(b) = \frac{\hat{D}_\infty(2b-2-r)}{r}. \tag{5.3}$$

Hence the stagnation condition $v(b) = 0$ is found to be equivalent to $b = 1+\frac{1}{2}r$, and under these circumstances a critical flow for large r is distinguished by $\hat{D}_\infty = 2/(2+r)^{\frac{1}{2}}$. Insertion of this expression in the criterion (5.2) yields:

$$r^2(\hat{\Psi}_1+\tfrac{1}{2})+2r(\hat{\Psi}_1+\tfrac{1}{2})+r\left(2-4\left(1-\frac{\Delta}{\hat{D}_\infty}\right)\right)+4 = 0.$$

This equation, valid for r approaching infinity, relates $\hat{\Psi}_1$, $\Delta/\hat{D}_\infty$, and r for the branch-point solutions under the auxiliary constraint that $v(b) = 0$, i.e. zero velocity on the right-hand side of the channel. By regarding r as the dependent variable and utilizing the fundamental prerequisite that this quantity be infinitely large as a consistency condition it is seen that $\hat{\Psi}_1 = -\frac{1}{2}$ implies $\Delta/\hat{D}_\infty = \frac{1}{2}$ for $r\to\infty$. Furthermore it is recognized that, given a large enough fixed value of r, $\Delta/\hat{D}_\infty = 0$ can only be realized for $\hat{\Psi}_1$ decreasing close enough to $-\frac{1}{2}$. Both of these features are clearly in evidence in figure 6, the former as the asymptotic behaviour of the separating curve for $\hat{\Psi}_1 = -\frac{1}{2}$, the latter as the growing magnitude of the intercept between the delimiting curve and the abscissa for decreasing $\hat{\Psi}_1$.

Since it has been argued elsewhere (Gill 1977) that $\hat{\Psi}_1 > 0$ may correspond to the geophysically most appropriate upstream flow distribution, the results summarized in figure 6 appear to indicate that, for the case of a parabolic bottom topography,

the applicability of orthodox hydraulic criteria for determining flow rates or upstream heights is mainly limited to narrow channels, i.e. small values of r. However beneficial this state of affairs may be for the utility of the perturbation expansions derived in the previous section, it nevertheless raises important questions concerning the aptness of the present theoretical framework for practical investigations. A discussion of this aspect of the problem is, however, deferred until the next section.

The investigation has so far almost entirely limited itself to an examination of the branch-point solutions. Since these, as previously discussed, determine the maximum discharge for a given upstream situation, they are undoubtedly of major interest from a theoretical as well as a practical standpoint. Care should, however, be taken to note also that the overall solutions as exemplified in figures 2 and 3 offer a general description of inviscid flow in a channel of varying topography under the assumption that the dynamical upstream parameters $\hat{D}_\infty$ and $\hat{\Psi}_1$ can be prescribed. It is furthermore important to emphasize that within this broader context, the occurrence of non-critical reversals of the flow can be interpreted in terms of blocking (cf. Røed 1980).

The problem treated by Røed differs from the one at hand in that he studied forced flows and moreover limited his attention to boundary currents with particular emphasis on how variations of the topography give rise to blocking. The somewhat different upstream conditions notwithstanding, it appears as though certain of the phenomena examined by Røed have counterparts within the framework of the present investigation. Hence it may be noted that for the general case of a very broad channel discussed above, there exists a parameter regime such that the supercritical branch of the limiting solutions (5.1a, b), is distinguished by the free surface having lost contact with the left-hand bank of the channel, i.e. $a \leqslant 0$. In these particular cases the supercritical channel flow assumes the characteristics of a boundary current subject to a slightly more complex bottom topography than the linear lateral slope considered by Røed in his special case when irregularities of the coastline are neglected. Taking advantage of formula (5.3) for the velocity on the right-hand side of the channel, it can furthermore be demonstrated that both blocked and unidirectional supercritical flow can occur within the parameter range where $a \leqslant 0$. Even though these features of the solutions (5.1a, b) have obvious counterparts within Røed's work, it must, however, be kept in mind that only a minor portion of his results can be reproduced by the present theory in the extreme of a very broad channel. It is, for instance, evident from expression (5.1a) that both the controlled and subcritical limiting solutions are invariably characterized by $a > 0$, a situation which precludes the existence of boundary currents in these cases.

6. Discussion

The aim of this study has been to extend the results of Gill (1977), valid for a rectangular geometry, to also encompass conditions in channels with continuously sloping side boundaries. This has proved feasible, and a unified mathematical treatment of the problem has been achieved. For a parabolic bottom profile it has been shown that the resulting algebraic problem can be resolved either using an iterative procedure or with a perturbation expansion.

One of the interesting conclusions which could be drawn from the calculations was that the possibility of resolving the discharge problem in terms of a controlled flow is somewhat limited in the case of a parabolic topography due to the vanishing depth of the fluid at the lateral boundaries. Nevertheless, for certain parameter regimes and

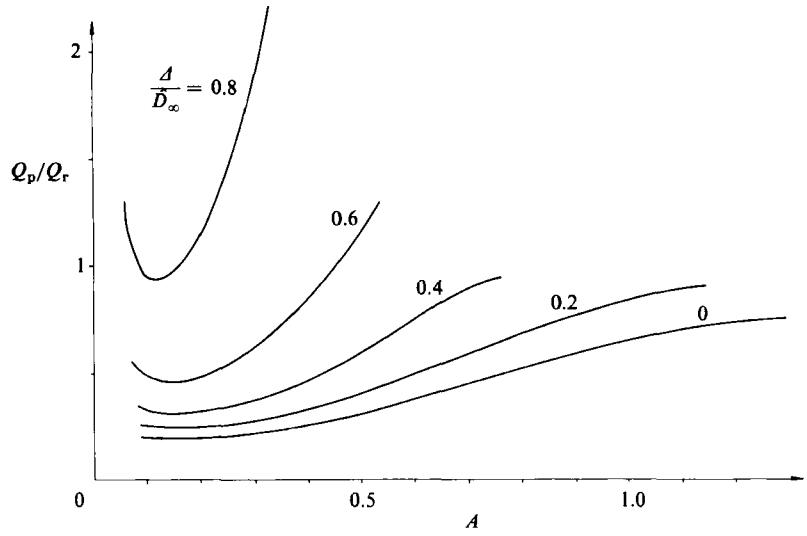

FIGURE 7. Q_p/Q_r, the ratio of the maximum flows in parabolic and rectangular channels, versus the area A for various values of the sill height $\Delta/\hat{D}_\infty$.

in particular for narrow constrictions, the notion of hydraulic control can serve as a useful tool for determining extremal flow properties. Since a parabolic cross-section is almost invariably a better approximation to conditions in nature than a rectangular one, it is of some interest to compare the controlled flow results derived here with those for the rectangular geometry.

An important difference between the two types of channel is that in the parabolic case the width of the flow is a dynamically determined variable, whereas for the rectangular geometry it can be regarded as prescribed. A comparison between the maximum flow rates for the two topographies has hence been undertaken for equal values of the cross-sectional area occupied by the flow. (This specific choice of comparative standard has the advantage that it eliminates the element of subjectivity associated with assigning a parabolic geometry with two degrees of freedom to a rectangular channel of given width.) For $\tilde{\Psi}_i = \frac{1}{2}$, figure 7 shows Q_p/Q_r, the ratio of the maximum flows in a parabolic and a rectangular channel respectively, versus the area A occupied by the flow for various values of $\Delta/\hat{D}_\infty$. All the curves start from a value of the cross-sectional area corresponding somewhat arbitrarily to a rectangular channel width of four hundredths of a Rossby radius. For $\Delta/\hat{D}_\infty = 0.4$, 0.6 and 0.8 the results are not shown beyond the point where the area represents a flow separated from the left-hand wall of the rectangular channel, since in this case the width of the channel is no longer relevant for the problem, which hence assumes the characteristics generally associated with inertial boundary currents (cf. Røed 1980). In a similar fashion the emergence of bi-directional flow associated with the branch-point solutions for a parabolic channel has been used as a termination criterion for $\Delta/\hat{D}_\infty$ equal to 0 and 0.2.

The overall results of the comparison, summarized in figure 7, indicate that for almost every situation, a rectangular channel yields the larger maximum flow. The difference is most pronounced for small areas and low sills, in which cases these flow rates can be up to five times larger than those for controlled flow in a parabolic channel.

The present investigation pertains to the somewhat specific case of a parabolic cross-sectional bottom profile of the channel. Nevertheless, the result indicating a limited parameter range compatible with hydraulic control in the established sense is undoubtedly generalizable to any topography with a continuously sloping bottom; this since the vanishing depth of the fluid at the horizontal extremes of the flow is a generic feature of such a geometry. From the standpoint of applying the present work to observations of strait flows in nature, where it is frequently conjectured that hydraulic control does occur, these restrictions may appear somewhat discouraging. (Not least does this holds true for the fact that the upstream conditions yielding the largest range of admissible geometrical parameters do not coincide with those postulated as being the most geophysically relevant ones.) It is, however, advisable to keep in mind that in any practical realization frictional effects can be expected to play an important role in regions of vanishing fluid depth. Thus it cannot be ruled out that in nature some type of quasi-inviscid control is established, even under conditions which, according to the strictly inviscid theory above, are only compatible with branch-points solutions involving flow reversals.

On might consider invoking friction in the formal treatment of the problem so as to ease the above-mentioned parameter restrictions. This course of action is, however, somewhat unattractive since it would not only constitute a violation of one of the fundamental tenets of hydraulic theory, but also give rise to an entirely different and more complex type of mathematical problem than the one examined here. With an eye to the future work it may thus be appropriate to conclude by noting that one way of extending the usefulness of the present theory appears to be through the introduction of a non-constant prescribed upstream potential vorticity. Hereby it should hopefully prove possible to realize uni-directional critical flow over the entire range of parameter values.

This work has been supported by the Swedish Natural Science Research Council under contract NFR-G-4768-103, which hereby is gratefully acknowledged. The authors are furthermore indebted to Dr A. E. Gill for valuable comments on a preliminary version of this manuscript.

Appendix. General recursive formulae

$$\begin{aligned}\delta(N):\ & 8a_0^3(a_{N-2}-b_{N-2})+12a_0^2(a_1+b_1)(a_{N-3}-b_{N-3})\\ & +12a_0^2(a_1-b_1)(a_{N-3}-b_{N-3})+2a_0(a_1-b_1)\sum_{k=1}^{N-4}(a_k+b_k)(a_{N-3-k}+b_{N-3-k})\\ & +4a_0(a_1+b_1)\sum_{k=1}^{N-4}(a_k-b_k)(a_{N-3-k}+b_{N-3-k})\\ & +4a_0^2\sum_{k=2}^{N-4}(a_k-b_k)(a_{N-2-k}+b_{N-2-k})+\sum_{l=2}^{N-4}\left[\sum_{k=0}^{l}(a_k-b_k)(a_{l-k}+b_{l-k})\right]\\ & \times\left[\sum_{k=0}^{N-2-l}(a_k+b_k)(a_{N-2-l-k}+b_{N-2-l-k})\right]\\ & +\sum_{q=4,\,6,\,\ldots}^{Q}[C_{q+1}\mathscr{A}(N-q,q+1)+\tfrac{1}{2}C_{q-1}\mathscr{A}(N-q,q-1)]/C_3=0,\end{aligned}$$

$$\sigma(N):\ 2(a_1-b_1)(a_{N-1}-b_{N-1})+2(a_2-b_2)(a_{N-2}-b_{N-2})+2a_0(a_{N-2}+b_{N-2})$$
$$+\sum_{k=3}^{N-3}(a_k-b_k)(a_{N-k}-b_{N-k})+\sum_{k=1}^{N-3}(a_k a_{N-2-k}+b_k b_{N-2-k})$$
$$+\sum_{q=4,6,\ldots}^{Q}\Big[2C_{q-1}\mathscr{B}(N-q,q)+4C_{q+1}\mathscr{B}(N-q,q+2)+\mathscr{B}(N-q,q-2)$$
$$\times\sum_{k=1,3,\ldots}^{q-3}C_kC_{q-2-k}+4\mathscr{B}(N-q,q)\sum_{k=1,3,\ldots}^{q-1}C_kC_{q-k}+4\mathscr{B}(N-q,q+2)$$
$$\times\sum_{k=1,3,\ldots}^{q+1}C_kC_{q+2-k}\Big]=0.$$

Here $\mathscr{A}(j,k)$ and $\mathscr{B}(j,k)$ denote the coefficients of p^j in the expansions of $(a-b)(a+b)^k$ and $(a+b)^k$ respectively. Q, the summation limit, is the integer part of $\frac{1}{2}N$ multiplied by two. The formulae are valid for $N \geqslant 6$.

REFERENCES

Gill, A. E. 1977 The hydraulics of rotating-channel flow. *J. Fluid Mech.* **80**, 641–671.

Hogg, N. G., Biscaye, P., Gardner, W. & Schmitz, W. J. 1982 On the transport and modification of the Antarctic Bottom Water in the Vema Channel. *J. Mar. Res.* **40** (Suppl.), 231–263.

Hogg, N. G. 1983 Hydraulic control and flow separation in a multi-layered fluid with applications to the Vema Channel. *J. Phys. Oceanogr.* **13**, 695–708.

Houghton, D. D. 1969 Effect of rotation on the formation of hydraulic jumps. *J. Geophys. Res.* **74**, 1351–1360.

Røed, L. P. 1980 Curvature effects on hydraulically driven inertial boundary currents. *J. Fluid Mech.* **96**, 395–412.

Sambuco, E. & Whitehead, J. A. 1976 Hydraulic control by a wide weir in a rotating fluid. *J. Fluid Mech.* **73**, 521–528.

Shen, C. Y. 1981 The rotating hydraulics of the open-channel flow between two basins. *J. Fluid Mech.* **112**, 161–188.

Stalcup, M. C., Metcalf, W. G. & Johnson, R. G. 1975 Deep Caribbean inflow through the Anegada–Jungfern Passage. *J. Mar. Res.* **33** (Suppl.), 15–35.

Stern, M. E. 1972 Hydraulically critical rotating flow. *Phys. Fluids* **15**, 2062–2064.

Stern, M. E. 1974 Comment on rotating hydraulics. *Geophys Fluid Dyn.* **6**, 127–130.

Van Dyke, M. 1974 Analysis and improvement of perturbation series. *Q. J. Mech. Appl. Maths* **27**, 423–450.

Whitehead, J. A., Leetmaa, A. & Knox, R. A. 1974 Rotating hydraulics of strait and sill flows. *Geophys. Fluid Dyn.* **6**, 101–125.